ACS APPLIED MATERIALS & INTERFACES

www.acsami.org

Research Article

Photo- and Humidity-Responsive Liquid Crystal Copolymer Actuators Fabricated via Vapor-Assisted Alignment

Haozhe Sun, Xingpeng Chai, Haipeng Yang, Jia Wei,* and Yanlei Yu

Cite This: *ACS Appl. Mater. Interfaces* 2024, 16, 15405−15415

Read Online

ACCESS | Metrics & More | Article Recommendations | Supporting Information

ABSTRACT: Deformable liquid crystal polymers (LCPs) driven by more than one external stimulus have received extensive attention in fields ranging from multifunctional soft robots to bionic actuators. Combining responsive liquid crystal with nonmesogenic responsive groups within polymer offers a versatile way to obtain multiresponsive LCPs. However, the incorporation of nonmesogenic responsive groups causes interruption in the assembly of mesogens and brings a challenge to the alignment of LCPs. Herein, a new method is put forward to facilitate uniform mesogen alignment by exerting water vapor in the film preparation process. Using this method, vapor-assisted alignment, the homeotropic alignment of azobenzene mesogens is achieved in a copolymer containing nonmesogenic poly(ethylene glycol) (PEG). The obtained copolymer films present photodeformation brought by azobenzene isomerization and humidity-responsive deformation resulting from the asymmetric swelling of film surfaces. The dual-responsive smart "blinds" and bionic flower actuators are fabricated to demonstrate the integration of the two different stimuli. This work is anticipated to provide a feasible alignment method for multiresponsive LCPs, showing the potential applications in soft robots, sensors, and biomimetic devices.

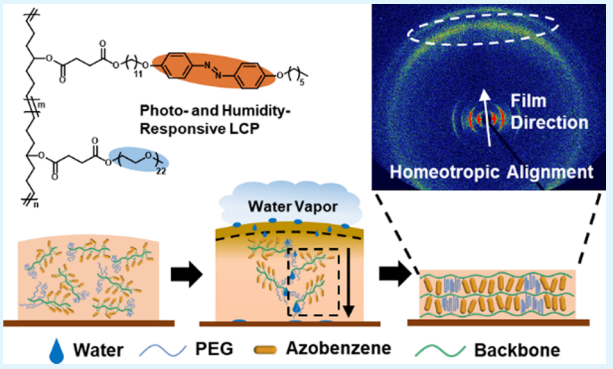

KEYWORDS: *liquid crystal polymer, photoresponsive, humidity-responsive, alignment, azobenzene*

1. INTRODUCTION

Deformable liquid crystal polymers (LCPs) have garnered tremendous attention because of their reversible deformation in response to a particular stimulus including light,[1−6] heat,[7−9] humidity,[10−15] electric,[16−20] magnetic field,[21−23] and so on. Furthermore, integrating multifaceted responsiveness into LCPs greatly enhances the versatility of these materials for the next-generation multifunctional actuators applied in changeable and complicated conditions.[24,25] Combining the nonmesogenic responsive groups with mesogens via copolymerization offers a feasible method to fabricate multiresponsive deformable LCPs. Generally, the deformation of LCPs depends on the ordered-to-isotropic alignment variation of the mesogens. However, introducing nonmesogenic groups into the LCP will disrupt the ordered structure of liquid crystal (LC) molecules and degrade the deformability of multiresponsive LCPs. Therefore, achieving the desired alignment of LC is a key step to obtain optimal deformation of LCPs, thereby allowing excellent actuation under different stimuli.

Nowadays, two main alignment methods have been devoted to obtain ordered LC structures in the multiresponsive deformable LCPs: the mechanical stretching/shear[26−30] and the topological/chemical surface anchoring effect.[31−35] In Yang and co-worker's work,[28] mechanical stretching was applied to align photo- and thermal-responsive polysiloxane LCP actuators. In response to light or thermal stimulation, the actuators shrank or bent along the stretching direction, mimicking the movement of starfishes. For another alignment method, our research group[36] first prepared photo- and humidity-responsive polyacrylate LCP films via photopolymerization of LC monomers and cross-linkers in LC cells with alignment layers, which guided the alignment of mesogens through surface anchoring effects. Schenning's team[37] demonstrated another dual-responsive LCP with splay alignment fabricated by surface anchoring, and photo- and humidity-responsive LCPs were constructed into bionic nocturnal flower actuators. These methods have some commonalities:[38] the LC monomers and oligomers are aligned before the polymerization/cross-linking. The good mobility of monomers and oligomers makes it convenient to guide the directions of the mesogens. After that, the monomers and oligomers are cross-linked to fix the orientation. However, the chemical cross-linked networks limit the remoldability and

Received: January 31, 2024
Revised: March 1, 2024
Accepted: March 5, 2024
Published: March 15, 2024

https://doi.org/10.1021/acsami.4c01809
ACS Appl. Mater. Interfaces 2024, 16, 15405−15415

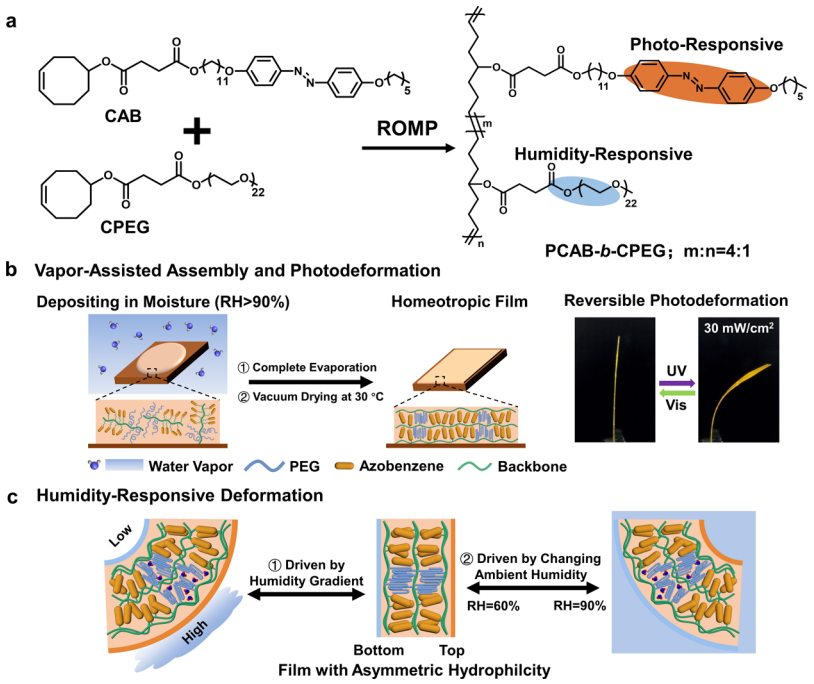

Figure 1. (a) Synthetic route of PCAB-*b*-CPEG via ROMP. (b) Schematic illustration of the fabrication of homeotropic alignment of LCP films via vapor-assisted alignment. The obtained films show reversible photoresponsive deformation under UV light irradiation (365 nm, 30 mW cm^{-2}) and visible light irradiation (530 nm, 50 mW cm^{-2}). Sample size: 10 mm × 3 mm× 20 μm. (c) Schematic illustration of humidity-responsive deformation driven by the humidity gradient and the changing ambient humidity.

recyclability of the obtained actuators, hindering the broader application of multiresponsive LCPs.

In addition, ordered LC structures can also be constructed through the self-assembly of side-chain LCPs,[39−41] which is a repeatable process exerted after polymerization. In our previous work,[42−45] several photodeformable linear LCPs derived from polycyclooctene were synthesized via ring-opening metathesis polymerization (ROMP). The layered smectic structures of these LCPs were easily fabricated via the spontaneous mesogen alignment in the thermal annealing process. Moreover, these linear LCPs were compatible with solution or melt processing, which made them convenient to produce 3D actuators,[42] combine with other materials[44] and be easily remolded or recycled. We also successfully adjusted the alignment of mesogens (in-plane or out-of-plane) by changing the length of the spacers, which also affected the photodeformation behaviors of LCPs.[43] Moreover, properly engineering the designable molecular structure via copolymerization enables the polycycloolefin-derived LCPs promising candidates to construct multistimuli-responsive LCPs. However, the self-assembly of LC molecules is sensitive to the adjacent groups, which means introducing new functional groups (especially nonmesogenic groups) into the polymer will disrupt the self-assembly of LC and hinder the deformation of multiresponsive LCPs.[46,47] As a result, it remains a great challenge to fabricate multiresponsive polycyclooctene LCPs via self-assembly.[48]

Herein, a novel method, vapor-assisted alignment, is put forward to fabricate a multiresponsive LC copolymer (PCAB-*b*-CPEG) bearing azobenzene mesogens and nonmesogenic poly(ethylene glycol) (PEG). Different from the homopolymer of azobenzene, the mesogens of copolymer (PCAB-*b*-CPEG) fail to align via self-assembly under thermal annealing due to the disturbance of PEG segments. Interestingly, we discover that exerting water vapor in the film fabrication process is an effective way to overcome the above drawback. To the best of our knowledge, this is the first work that facilitates the alignment of the LC via introducing water vapor. With the help of this alignment method, PCAB-*b*-CPEG films form homeotropic LC alignment and perform reversible photodeformation behaviors under UV/visible light irradiation. The obtained films also exhibit humidity-responsive bending, which is activated by the gradient humidity field or the changed ambient humidity. Furthermore, actuators of bionic flowers and self-adaptation "blinds" are prepared to demonstrate the photo- and humidity-responsiveness of PCAB-*b*-CPEG, especially their reversible, programmable, precisely controlled shape-changing behaviors.

2. RESULT AND DISCUSSION

2.1. Preparation of Photo- and Humidity-Responsive Copolymers Films via Vapor-Assisted Alignment. To combine the photo- and humidity-responsiveness, a block copolymer PCAB-*b*-CPEG was synthesized by the copolymerization of azobenzene and PEG-containing monomers (CAB and CPEG) via ROMP (Figure 1a). Monomer CAB was prepared according to the previous work,[42] while CPEG was synthesized with a similar route and characterized by ^{1}H NMR (Figure S1 in Supporting Information). Copolymer PCAB-*b*-CPEG showed the number-average molecular weight (M_n) of 1.7 × 10^5 g mol^{-1} with the molar composition ratio of 4:1 (CAB to CPEG) as evidenced by ^{1}H NMR and gel permeation chromatography (GPC) (Figures S2 and S3a in Supporting Information). Azobenzene mesogens are anticipated to endow the PCAB-*b*-CPEG with liquid crystallinity and serve as photoresponsive groups. On the other hand, the hygroscopic PEG component provides the copolymer with swellability to perform humidity-responsive deformation. The ratio of the two

https://doi.org/10.1021/acsami.4c01809
ACS Appl. Mater. Interfaces 2024, 16, 15405−15415

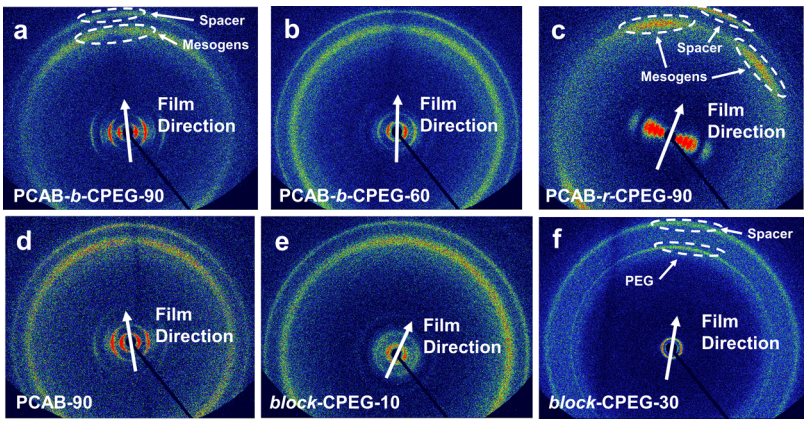

Figure 2. 2D-WAXD images of films: (a) PCAB-*b*-CPEG-90, (b) PCAB-*b*-CPEG-60, (c) PCAB-*r*-CPEG-90, (d) PCAB-90, (e) *block*-CPEG-10, and (f) *block*-CPEG-30.

components is very important as a trade-off between liquid crystallinity and multifunctionalization. In the experiments, we discovered that PCAB-*b*-CPEG with a molar ratio of 4:1 (CAB to CPEG) exhibited the right balance. The polarizing optical microscope (POM) images demonstrated that PCAB-*b*-CPEG showed the texture of an LC at 20 °C, and the transition temperature from the LC state to the isotropic state was around 80 °C (Figure S3b in the Supporting Information).

The alignment of liquid crystalline plays a vital role in the photodeformation of LCP. In our previous studies, the polycycloolefin photoresponsive LCP (homopolymer of CAB) showed excellent photodeformation by virtue of the self-assembled LC structures obtained through thermal annealing.[42] However, with the same preparation process, the obtained PCAB-*b*-CPEG films hardly exhibited an aligned LC structure nor photodeformation, which implied that the thermal annealing failed to overcome the interruption of nonmesogenic groups on the self-assembly of LC. Therefore, a new method was attempted to facilitate the self-organization of mesogens by introducing water vapor into the film preparation. As shown in Figure 1b, the PCAB-*b*-CPEG solution was drop-cast on glass substrates to form films under 90% relative humidity (RH). The obtained LCP films are designated as PCAB-*b*-CPEG-X and X corresponds to the surrounding RH in the preparation process. Fortunately, we found that the films prepared under 90% RH (PCAB-*b*-CPEG-90) performed stable and reversible photoresponsive behaviors, which indicated the feasibility of the new vapor-assisted method. In addition, the PCAB-*b*-CPEG-90 films performed two humidity-responsive deformation modes driven by the humidity gradients and the changed ambient humidity, respectively (Figure 1c), which will be discussed later in detail.

The mesogen alignment of PCAB-*b*-CPEG-90 films was characterized by two-dimensional wide-angle X-ray diffraction (2D-WAXD). As shown in Figure 2a, the diffraction arcs in the low-angle region appeared on the equator line, implying the formation of a smectic phase with the normal direction of smectic layers perpendicular to the film plane. In the high-angle region, two diffraction arcs on the meridian featured the homeotropic alignment of mesogens in the smectic A phase. Then, the effects of heating on the mesogen order of the PCAB-*b*-CPEG-90 film were examined by 2D-WAXD (Figure S11b,c in the Supporting Information). The 2D-WAXD images show that the PCAB-*b*-CPEG-90 film still maintained smectic A structures after the film was heated to 60 °C, while the film experienced a significant loss of order at an LC-to-isotropic phase transition temperature of 90 °C.

The influence of humidity during preparation on the alignment of PCAB-*b*-CPEG films was also evaluated. None of the films prepared under lower humidity (60−80% RH) exhibited uniform alignment (as evidenced in Figure S4 in Supporting Information). Typically, the 2D-WAXD of PCAB-*b*-CPEG-60 showed diffraction rings in the high-angle region (Figure 2b), indicating the disordered mesogen structures. As suggested above, the uniform homeotropic alignment only appeared when the films were prepared under high humidity (90% RH).

The random copolymer (PCAB-*r*-CPEG, the "*r*" denoting random) was prepared to obtain a view of the applicability of the vapor-assisted alignment. PCAB-*r*-CPEG has the same component ratio of 4:1 (CAB to CPEG) as PCAB-*b*-CPEG (evidenced by ^{1}H NMR, Figure S5 in the Supporting Information). As shown in Figure 2c, PCAB-*r*-CPEG-90 films prepared under high humidity presented the homeotropic alignment with a smectic C structure. The effects of heating on the mesogen order of PCAB-*r*-CPEG-90 film were also examined by 2D-WAXD (Figure S11d,e in the Supporting Information). The PCAB-*r*-CPEG-90 underwent a phase transition from smectic C to smectic A at 60 °C and an isotropic transition around 85 °C. Furthermore, we prepared a film of PCAB-*r*-CPEG-90 with a thickness of 50 μm and evaluated alignment using 2D-WAXD (Figure S10 in the Supporting Information). The PCAB-*r*-CPEG-90 film with 50 μm thickness exhibited clear alignment with smectic C structure, which was similar to that of the film with 20 μm thickness (Figure 2c). These experimental results confirmed that the vapor-assisted alignment was effective both to random and block copolymer, and thicker film cast through the vapor-assisted approach could still achieve the desired alignment.

On the contrary, the vapor-assisted alignment is unsuitable for the homopolymer of CAB (PCAB). As shown in Figure 2d, the diffraction rings in the high-angle region of the 2D-WAXD images of PCAB-90 reflected the disordered alignment of the mesogens. This observation suggested that the existence of PEG units was indispensable in the alignment method. Copolymers with different content of CPEG were prepared to investigate the influences of PEG on the alignment of copolymer films. As mentioned above, the molar composition ratio of PCAB-*b*-CPEG-90 is 4:1 (CAB to CPEG), implying that this block copolymer contains 20 mol % of CPEG. For

https://doi.org/10.1021/acsami.4c01809
ACS Appl. Mater. Interfaces 2024, 16, 15405−15415

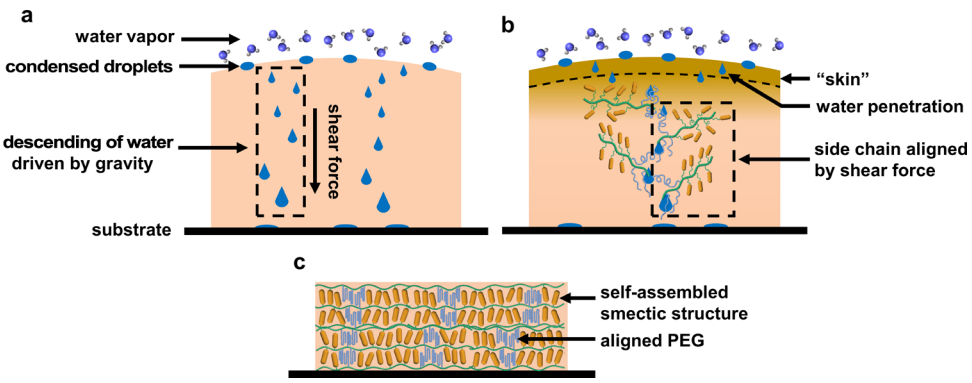

Figure 3. Schematic illustrating the mechanism of vapor-assisted alignment. (a) Water vapor condenses on the surface of toluene solution and descends into the solution by gravity, creating vertical shear force. (b) Polymer "skin" containing the PEG component is formed with the evaporation of solvent. Water droplets would penetrate the "skin" and enter the solution continuously, assisting the alignment side chains of the copolymer. (c) With the complete evaporation of toluene solvent, the self-assembled smectic structure is fixed.

comparison, we prepared two other block copolymer films with 10 mol % CPEG (*block*-CPEG-10) and 30 mol % (*block*-CPEG-30) by vapor-assisted alignment. As illustrated in Figure 2e, 2D-WAXD of the *block*-CPEG-10 film showed uniform diffraction rings in the high-angle region, indicating the absence of aligned LC structures. This result highlights the necessity of adequate PEG content for effective alignment.

As the CPEG content increased to 30 mol %, the diffraction signal of azobenzene mesogens became completely dispersed (Figure 2f). This indicated that *block*-CPEG-30 lost liquid crystallinity due to the excess of the PEG component. Conversely, a clear diffraction arc corresponding to crystallized PEG was observed, suggesting the alignment of PEG side chains via the vapor-assisted alignment process. On the basis of the above results, we found that both azobenzene and PEG were able to align during vapor-assisted preparation, and the spacers of all oriented LCPs were also oriented (Figure 2a,c,f).

To demonstrate that the alignment is predominantly governed by the vapor-assisted alignment rather than occurring during the fast evaporation of water in vacuum drying, we compared the 2D-WAXD of the PCAB-*r*-CPEG-90 film as-prepared via a vapor-assisted process (Figure S9 in the Supporting Information) with that of the film subjected to vacuum drying following the vapor-assisted process (Figure 2c). The analogous X-ray diffraction patterns indicated that the film prepared through the vapor process already exhibited good orientation, whereas the orientation remained unaffected by the vacuum drying process, suggesting that the alignment was induced during the vapor-assisted preparation process. Meanwhile, the film of PCAB-*r*-CPEG prepared under 60% RH was put in the humidity chamber with 90% RH for 2 h. The photodeformability of the sample before and after exposure to 90% RH was assessed (see Figure S15 in Supporting Information). None of the samples performed reversible photodeformation. This experiment also proved that the alignment of mesogen is minimally affected by water vapor once the film preparation is completed. In summary, subjecting the film to high humidity or removing water from it at low temperatures did not affect the alignment of LC. Thus, it is reasonable to infer that the alignment process primarily occurred in the presence of toluene, and the alignment is not dependent on the water absorbed by the sample.

Based on the above results, we postulate that the downward movement of water plays a pivotal role in guiding the self-assembly of LCP. As shown in Figure 3, the descending of water happens in two phases. Initially, water droplets condense on the solution surface because of the temperature reduction caused by the evaporation of the toluene solvent. Subsequently, they descend into the solution under the influence of gravity (Figure 3a). As toluene evaporates, a thin polymer layer forms on the solution surface, termed the polymer "skin". Sufficient PEG contents within the polymers facilitate continuous entry of water droplets into the solution through the polymer "skin" in high humidity conditions (Figure 3b). The shear force induced by water movement promotes the alignment of side chains of LCP. We think there are two possible pathways for the shear force of water to affect azobenzene. When PEG experiences downward water shearing, adjacent azobenzene may also undergo shearing induced by water. Alternatively, the downward movement of water in the solution impels the surrounding toluene solution to move, thereby influencing the alignment of azobenzene within the solution. Finally, with solvent evaporation, the LCP solution solidifies to a film, and the homeotropic alignment of mesogens is fixed (Figure 3c).

It is noteworthy that the PEG content significantly influences the vapor-assisted alignment. For copolymers containing adequate PEG content (≥20 mol %, such as PCAB-*b*-CPEG-90), the hygroscopic skin facilitated water penetration through the "skin" into the solution. The shear force generated by ongoing water penetration aids in aligning both the azobenzene molecules and PEG side chains. Conversely, low PEG content (<20 mol %) in the polymer impedes water droplet entry through the skin, thereby hindering vapor-assisted alignment.

2.2. Photo-Responsive Deformation of LCP Copolymer Films. The photoresponsive deformation of the aligned PCAB-*b*-CPEG films was investigated under 365 nm UV light and 530 nm visible light. As shown in Figure 4a, the PCAB-*b*-CPEG-90 film exhibited reversible bending under light stimulation. Upon UV light irradiation, the *trans*-to-*cis* isomerization of azobenzene triggers the alignment variation from homeotropic to isotropic, leading to local expansion on the surface and bending away from the light source. The film is restored to its initial shape upon irradiation of visible light with the *cis*-to-*trans* isomerization of azobenzene (Movie S1 in Supporting Information). We further assessed the photothermal effect of the films under different intensities of UV/visible light irradiation (see Figure S11, Supporting Information). The results showed that the PCAB-*b*-CPEG-90 film

https://doi.org/10.1021/acsami.4c01809
ACS Appl. Mater. Interfaces 2024, 16, 15405−15415

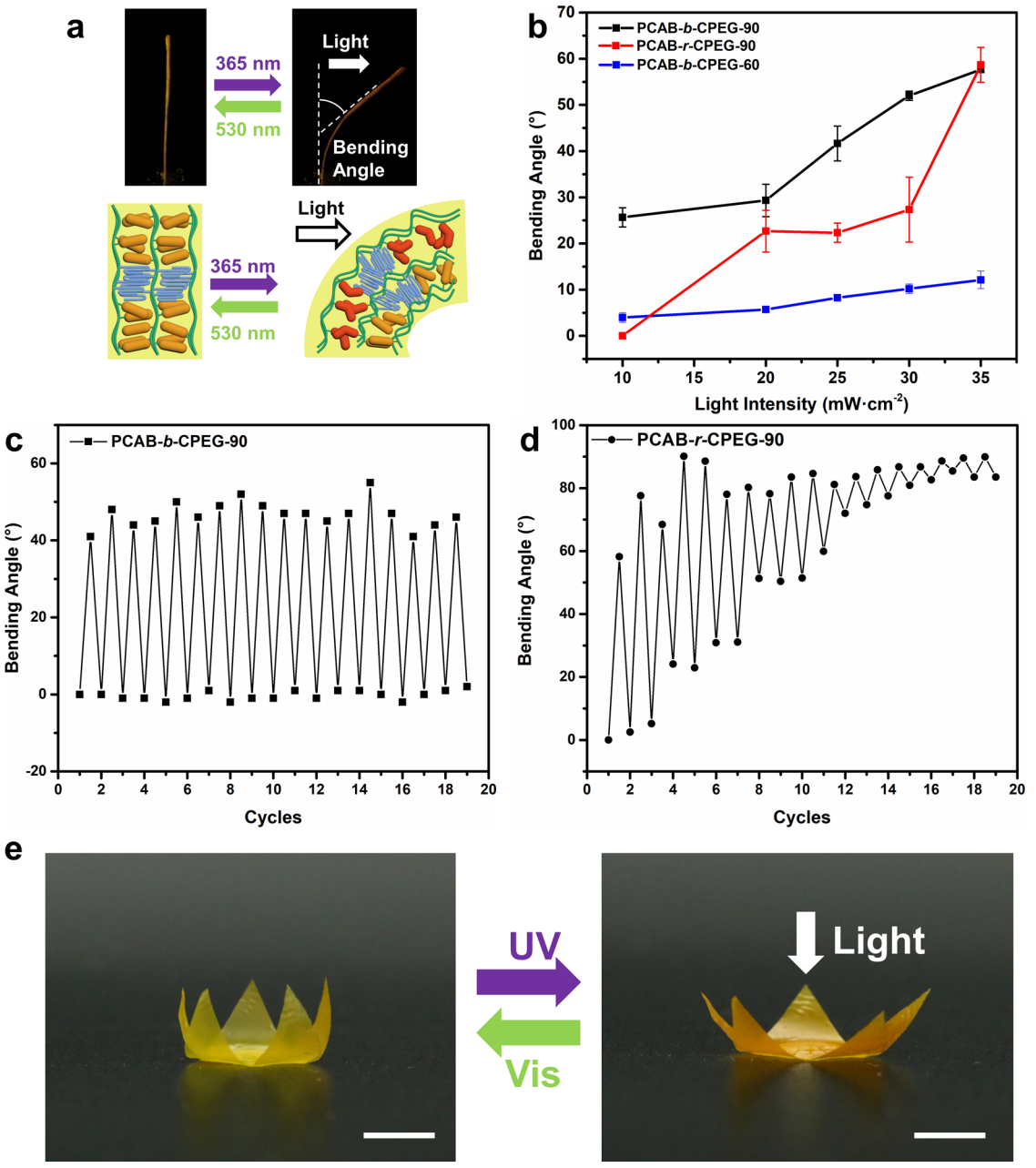

Figure 4. (a) Images of photoresponsive deformation of PCAB-*b*-CPEG-90 films (sample size: 10 mm × 3 mm × 20 μm) and the schematics illustration of the alignment variation of mesogens under UV/visible light irradiation. (b) Curves of bending angle as a function of UV light intensity (wavelength: 365 nm). Cyclic performance of (c) PCAB-*b*-CPEG-90 and (d) PCAB-*r*-CPEG-90 films under alternative irradiation of UV (365 nm, 30 mW cm^{-2}) and visible light (530 nm, 50 mW cm^{-2}). (e) Photodeformation and recovery of the PCAB-*b*-CPEG-90 flower actuator. Scale bar: 5 mm.

attained the maximum temperature of 35 °C under the illumination of 50 mW cm^{-2} UV light, which is lower than the isotropic transition temperature of the LC copolymer. Therefore, the photodeformation of PCAB-*b*-CPEG-90 is not prompted by a photothermal-induced phase transition. Then, we quantified the photodeformation behaviors of different LCP films by bending angles, as depicted in Figure 4b. The bending angles of PCAB-*b*-CPEG-90 and PCAB-*r*-CPEG-90 films with homeotropic alignment increased with increasing light intensity at 365 nm and reached the maximum of 60° when exposed to 35 mW cm^{-2} UV light. Conversely, the PCAB-*b*-CPEG-60 film with disordered alignment underwent maximum photodeformation of only 10° upon exposure to UV irradiation. The significant differences in responsive behaviors are ascribed to the alignment of LC molecules.

To further analyze the photoresponsive deformation of PCAB-*b*-CPEG-90 and PCAB-*r*-CPEG-90 films, the cycling performances of photodeformation were studied by irradiating the two films with UV (365 nm, 30 mW cm^{-2}) and visible light (530 nm, 50 mW cm^{-2}) alternately. After 20 irradiation cycles, the maximum bending angle of PCAB-*b*-CPEG-90 films remained almost unchanged, reflecting excellent antifatigue performance (Figure 4c). On the contrary, the deformation angle of PCAB-*r*-CPEG-90 films started to decrease in the fourth cycle and lost the deformability in the 12th cycle, indicating the creep of polymer chains in deformation (Figure

https://doi.org/10.1021/acsami.4c01809
ACS Appl. Mater. Interfaces 2024, 16, 15405−15415

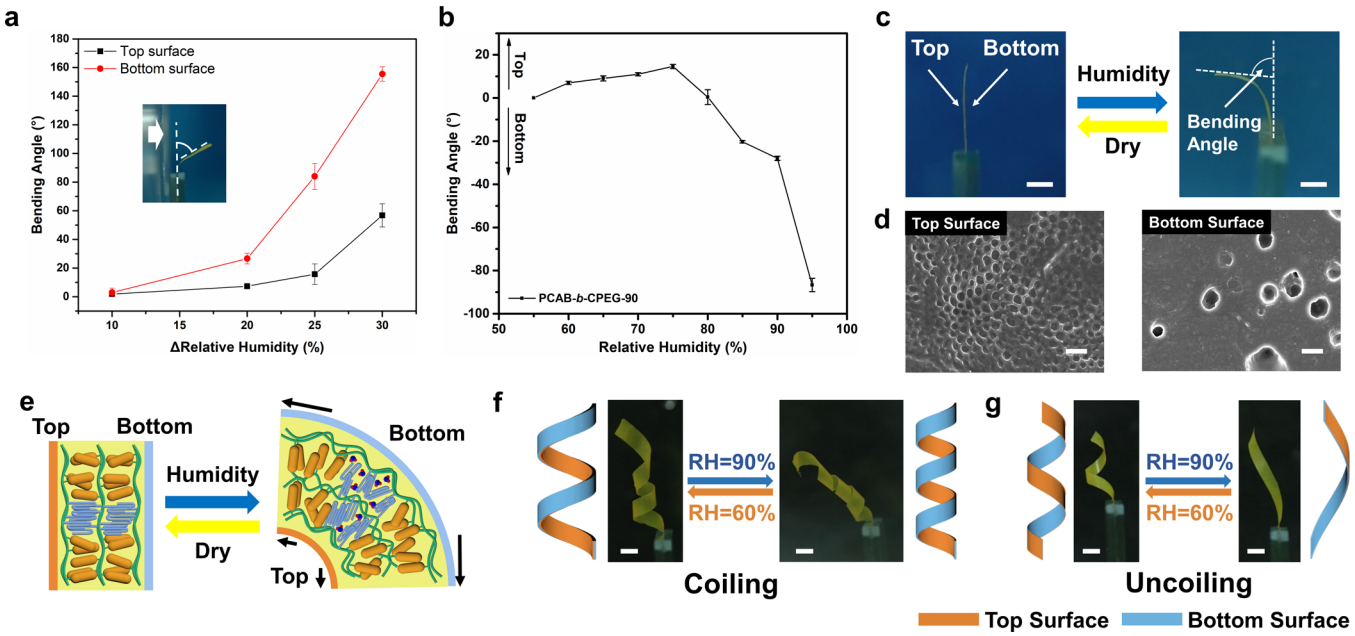

Figure 5. (a) Bending angles of PCAB-*b*-CPEG-90 films under different humidity gradients. The bottom surface of PCAB-*b*-CPEG-90 showed greater responsive deformation when subjected to the humidity gradient. Inset: Image of the responsive behavior of the films under humidity gradient. The size of the sample is 8 mm × 2 mm × 20 μm. The arrow represents the direction of the moisture source. (b) Relationship between ambient humidity and bending angles for PCAB-*b*-CPEG-90 films. Positive and negative bending angles mean the films bend toward the bottom surface and top surface, respectively. (c) Illustration of directional deformation for PCAB-*b*-CPEG-90 in changing ambient humidity. The size of the sample is 8 mm × 2 mm × 20 μm. Scale bar: 2 mm. (d) SEM images of the top and bottom surface of PCAB-*b*-CPEG-90 films. The bottom surface was smoother than the top surface, which contributed to better hydrophilicity. Scale bar: 1 μm. (e) Schematic showing the mechanism of directional humidity-responsive deformation in changing ambient humidity. The samples were twisted into spirals through thermal processing with the bottom surface (f) outside and (g) inside the spiral, possessing different deformation behaviors under humidity stimulation. Scale bar: 2 mm.

4d). We also conducted the 2D-WAXD to investigate the change of mesogen alignment and the order parameter before and after cyclic deformation (Figure S13, Supporting Information). Before the deformation, two diffraction arcs in the high-angle region are observed clearly; the order parameter before deformation is 0.63. After 20 cycles, the diffraction signals at high-angle regions became more dispersed, resulting in a reduction of the order parameter to 0.58.

The differences are closely related to the lamellar smectic structure of azobenzene mesogens and the crystallization of PEG segments, which both serve as physical cross-links to prevent the creep of polymer chains during deformation. The LC structure and the melting enthalpy for PEG were characterized by one-dimensional X-ray diffraction (1D-XRD) and differential scanning calorimetry (DSC), as shown in Figures S6 and S7 in the Supporting Information. According to the 1D-XRD results, the layer spacing of lamellar smectic structures of PCAB-*b*-CPEG-90 was 4.6 nm, smaller than that of PCAB-*r*-CPEG-90 (8.0 nm), which was ascribed to the improved phase separation between PEG and azobenzene endowed by the block structure. The tense layered smectic structures act as strong physical cross-links to prevent the creep of polymer chains in deformation. Simultaneously, the melting point and melting enthalpy of PEG in PCAB-*b*-CPEG-90 were higher than that of PCAB-*r*-CPEG-90 as calculated from DSC (Figure S7 in Supporting Information), reflecting the better crystallization of PEG segments. Therefore, the smaller layer spacing of lamellar structures and the high melting enthalpy of PEG of PCAB-*b*-CPEG-90 indicate the existence of stronger physical cross-links in the films and guarantee excellent antifatigue performance. Furthermore, the crystallized PEG segments would not be disturbed by the photoisomerization of azobenzene groups. Moreover, the melting point of PEG crystal is about 40 °C, which is higher than the maximum temperature of the material (35 °C) under UV light irradiation (See Figure S11a, Supporting Information). Thus, most crystallized PEG would remain stable during photodeformation and serve as physical cross-links.

A photoresponsive artificial flower actuator was constructed to demonstrate the photodeformation of PCAB-*b*-CPEG-90 films. As shown in Figure 4e, the petals and the floral disc of the actuators were tailored from a piece of film and combined together. The flower actuator opened upon exposure to UV light and restored to its initial shape under visible light, showing the reversible photoresponsive deformation of PCAB-*b*-CPEG-90 films (Movie S2 in Supporting Information).

2.3. Humidity-Responsive Deformation of LCP Copolymer Films. Besides the photoresponsive deformation enabled by azobenzene mesogens, PCAB-*b*-CPEG-90 also possessed sufficient hygroscopicity to perform reversible humidity-responsive deformation. During humidity-responsive deformation, the amorphous PEG segments primarily facilitate deformation by absorbing water from the surrounding air. Simultaneously, the ordered LC structures and part of the crystallized PEG segments served as physical cross-links, ensuring the reversibility of humidity-responsive deformation. Once moisture approaches one side of the film, the asymmetric swelling of the surface induces the bending under humidity gradients. Figure 5a shows the bending angle of the PCAB-*b*-CPEG-90 film when the top side or bottom side of the film was subjected to humidity. As the top side was subjected to humidity gradients, the bending angles of PCAB-*b*-CPEG-90

https://doi.org/10.1021/acsami.4c01809
ACS Appl. Mater. Interfaces 2024, 16, 15405−15415

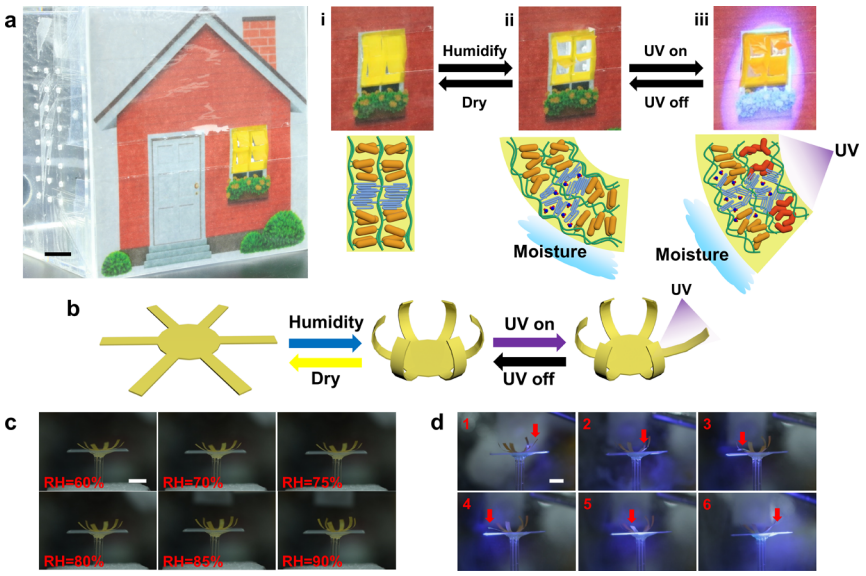

Figure 6. (a) Image of a "house" with a PCAB-*b*-CPEG-90 film as smart "blinds". Illustration of (i) close and (ii) open of blinds driven by humidity gradient. (iii) The self-regulation of blinds under stimulation of both light and humidity. Size of the film: 20 mm × 15 mm × 20 μm. Scale bar: 5 mm. (b) Schematic illustration of the dual-responsive deformation of artificial flower. (c) Side view of humidity-responsive deformation of artificial flower actuator. The flower actuator closed in response to the increasing humidity, showing the global control through humidity stimulation. Scale bar: 5 mm. (d) Side view of photoresponsive of artificial flower actuators. Only the pedal illuminated with UV light opened (marked with red arrow), demonstrating the local control of light stimulation. Scale bar: 5 mm. (wavelength: 365 nm).

films gradually increased from 10 to around 50° as the humidity gradients (ΔRH) between the two sides surrounding the film increased from 20 to 30%. However, when the bottom surface was subjected to humidity gradients, the bending angles of the PCAB-*b*-CPEG-90 film were up to 160° as the ΔRH reached 30%. This phenomenon inspired us to further investigate the humidity-responsive properties of PCAB-*b*-CPEG-90.

In addition to the bending behavior under a humidity gradient, humidity-responsive bending can also be realized by exposing asymmetric films to uniformly changed ambient humidity. Generally, asymmetric films are obtained by constructing a bilayer structure or applying a selective surface treatment.[11,49] To our surprise, we found that the monolithic PCAB-*b*-CPEG-90 films also deformed by uniformly changing the surrounding moisture. As shown in Figure 5b,c, the bending angles of PCAB-*b*-CPEG-90 films increased with the increasing surrounding humidity, and the maximum deformation angle was 90° when the ambient humidity reached 95% RH. This behavior is attributed to the asymmetric hydrophilicity between two surfaces of PCAB-*b*-CPEG-90 films, which was proved by static water contact angles (CA) of the top and bottom surfaces (see Figure S8 in the Supporting Information). The bottom surface of PCAB-*b*-CPEG-90 films (CA:83.0 ± 2.4°) was more hydrophilic than the top surface (CA:95.8 ± 4.4°). To further investigate the asymmetric hydrophilicity, the morphology of PCAB-*b*-CPEG-90 films was studied by SEM, as shown in Figure 5d. According to the images, the bottom surface of PCAB-*b*-CPEG-90 films was smoother than that of the top surface. During the vapor-assisted alignment, the condensed water droplets cause honeycomb-like structures, which also increase the CA of the top surface. When the PCAB-*b*-CPEG-90 films are exposed to moisture, the bottom surface absorbs more water than the top surface, resulting in asymmetric swelling and the bending of the film under homogeneous ambient humidity, as illustrated in Figure 5e.

Since the humidity-responsive deformation of PCAB-*b*-CPEG-90 under changing humidity depends on asymmetric hydrophilicity, it is feasible to design the deformation behaviors of actuators by adjusting the aspects of the top and bottom surfaces. Therefore, two spiral actuators with opposite surface aspects were fabricated to display the control of the deformation. As shown in Figure 5f, the spiral actuator curled in high humidity when the bottom surface was facing outward (Movie S3 in Supporting Information). On the contrary, if the bottom surface faced toward the axis of the spiral, the actuator uncurled in the increasing ambient humidity (Figure 5g and Movie S4 in Supporting Information).

2.4. Dual-Responsive Actuators of PCAB-*b*-CPEG. The PCAB-*b*-CPEG-90 films are sensitive to both light and humidity, offering an opportunity to develop soft actuators applied in changeable and complicated conditions. Therefore, smart actuators were constructed to demonstrate the responsive deformation of copolymer through multiple tuning ways. We designed self-regulated "window blinds" that can open and close under light and humidity stimulation, as illustrated in Figure 6a and Movie S5 in the Supporting Information. When humidity inside the "house" increased, the "blinds" rolled up to release moisture (Figure 6i,ii). Meanwhile, UV irradiation from outside activated the photodeformation of the film and made the blinds fall down to block the "sunlight" (Figure 6iii). Under the simultaneous stimuli, the humidity-responsive rolling-up and the photoresponsive falling-down of blinds were in equilibrium, showing the smart deformation behaviors of PCAB-*b*-CPEG-90 films in response to complicated conditions.

A combination of different tuning methods is an important approach to achieve programmable actuators. Therefore, a dual-responsive artificial flower with six petals was fabricated to

https://doi.org/10.1021/acsami.4c01809
ACS Appl. Mater. Interfaces 2024, 16, 15405−15415

illustrate the combination of local UV irradiation and global humidity stimulation by recycling the remnants of the blind actuator, as illustrated in Figure 6b. With the increasing humidity, all of the petals gradually closed, demonstrating the control of the global shape of actuators (Figure 6c and Movie S6 in Supporting Information). Meanwhile, upon local irradiation with 365 nm light, the irradiated pedal bent backward while the other pedals remained unchanged, which showed precise programmable control on the local movement of actuators (Figure 6d and Movie S7 in Supporting Information). Overall, the programmable and tailorable deformation in response to two different tuning ways was demonstrated, which can be utilized in dual-responsive smart devices. Finally, since the PCAB-*b*-CPEG-90 does not have chemical cross-links, it is easy to recycle and reprogram the actuators using the same film via the solution process. In fact, the remnants of the smart "blind" actuator were dissolved in toluene and reprocessed to a new film through a vapor-assisted process, which was used to fabricate the dual-responsive artificial flower. Therefore, if the actuators were damaged or the alignment of the material is disturbed by heating, we can dissolve the damaged materials in the proper solvent and reproduce the film via vapor-assisted alignment easily.

3. CONCLUSIONS

In summary, we prepare a photoresponsive and humidity-responsive polycycloolefin LCP by copolymerizing azobenzene- and PEG-containing monomers via ROMP. A new method, vapor-assisted alignment, is utilized to overcome the disruption of nonmesogenic groups in the self-organization of LC molecules. A micro amount of water condensed from vapor is introduced into the LCP solution deposition process to provide downward shear force for the homeotropic alignment of mesogens, enabling the photoresponsive deformation of PCAB-*b*-CPEG films. In addition, the asymmetric PCAB-*b*-CPEG-90 films possess two humidity-responsive deformation modes: deformation under a humidity gradient and under changing ambient humidity. Afterward, smart "blinds" and artificial flower actuators are fabricated to illustrate the integration of photo- and humidity-responsive deformation into the single LCP.

This work provides a convenient method to address the disturbance of the nonmesogenic group on the self-assembly of mesogens in dual-responsive LC copolymers. Compared with the traditional alignment methods, the vapor-assisted alignment of LC is carried out after polymerization and does not require chemical cross-linking to fix the alignment. Looking forward, vapor-assisted alignment may serve as a universal alignment method for the multifunctional LCPs containing different nonmesogenic groups by changing the types of solvent vapor. We anticipate that the vapor-assisted alignment could offer more chances for the combination of mesogenic and nonmesogenic responsive groups to construct multifunctional LCP actuators for applications in soft robots, sensors, and biomimetic devices.

4. EXPERIMENTAL SECTION

4.1. Materials. 5-Cyclooctene-1-succinic ester (95%) was received from Chemsoon Co., Ltd.; poly(ethylene glycol) monomethyl ether 1000 (CP, mPEG-1000) was purchased from Tokyo Chemical Industry (TCI). 4-Dimethylaminopyridine (99%, DMAP), dicyclohexylcarbodiimide (99%, DCC), tetrahydrofuran (99%, THF), dichloromethane (AR, DCM), ethyl vinyl ether (98%, EVE), and methanol (99%) were obtained from Adamas. Second-generation Grubbs catalyst (98%) was purchased from Sigma-Aldrich. Anhydrous diethyl ether (AR) was purchased from Changshu Hongsheng Fine Chemical Industry Co., Ltd.; toluene (AR) was purchased from Shanghai Dahe Chemical Co., Ltd. DCM was purified by distillation over CaH_2. Other reagents were used as received unless otherwise noted.

4.2. Synthesis of the Monomers. The azobenzene-containing monomer (CAB) was prepared according to the published work.[42] Synthesis of PEG-containing monomer (CPEG): 5-cyclooctene-1-succinic ester (1.3 g, 6 mmol), mPEG-1000 (4.0 g, 4 mmol), and DMAP (0.5 g, 4 mmol) were added into a 500 mL flask and dissolved by 100 mL of THF. Then, DCC (2.5 g, 12 mmol) was dissolved in 50 mL of THF and added to the mixture dropwise. The mixture was stirred for 72 h at ambient temperature and filtrated to remove the precipitates. THF solvent was removed under reduced pressure; the condensed reaction mixture was dissolved in a small amount of DCM, precipitated from ice-cold anhydrous diethyl ether, and dried under vacuum overnight. The white solid monomer CPEG was obtained (3.5 g, 72%). ^{1}H NMR (400 MHz, $CDCl_3$, δ): 5.68 (m, 2H), 4.85 (m, 1H), 4.26 (t, 2H), 3.74−3.64 (m, 84H), 3.58 (m, 2H), 3.40 (s, 3H), 2.63 (m, 4H), 2.40−1.55 (m, 10H).

4.3. Synthesis of Block Copolymer PCAB-*b*-CPEG. The copolymerization of CAB and CPEG was performed by using standard Schlenk techniques under an argon atmosphere. CAB (0.20 g, 0.30 mmol) was first placed in a Schlenk flask. Then, a second-generation Grubbs catalyst (0.63 mg, 0.75 μmol) dissolved in 0.30 mL of anhydrous DCM was added. After stirring for 90 min at 50 °C, CPEG (0.09 g, 0.075 mmol) with 0.10 mL of anhydrous DCM was added to the mixture. The mixture was continually stirred at 50 °C for another 3 h. After polymerization, the concentrated reaction mixture was dissolved in DCM and 0.50 mL of EVE was added to quench the reaction. The product was purified via precipitation in methanol and dried under a vacuum overnight (0.22 g, 75%). ^{1}H NMR (400 MHz, $CDCl_3$, δ): 7.88 (d, 3.2H), 7.01 (d, 3.2H), 5.37 (d, 2H), 4.90 (s, 1H), 4.26 (t, 0.4H), 4.04 (m, 4.8H), 3.74−3.64 (m, 16.8H), 3.58 (m, 0.4H), 3.40 (s, 0.6H), 2.63 (m, 4H), 2.10−1.20 (m, 20.8H), 0.93 (t, 2.4H).

4.4. Synthesis of Random Copolymer PCAB-*r*-CPEG. The copolymerization of CAB and CPEG was performed using standard Schlenk techniques under an argon atmosphere. CAB (0.20 g, 0.30 mmol) and CPEG (0.09 g, 0.075 mmol) were added into a Schlenk flask. Then, a second-generation Grubbs catalyst (0.63 mg, 0.75 μmol) with 0.40 mL of anhydrous DCM was added. After stirring for 90 min at 50 °C, the reaction mixture was dissolved in DCM, and 0.50 mL of EVE was added to quench the reaction. The product was purified via precipitation in methanol and dried under a vacuum overnight (0.23 g, 80%).

4.5. Preparation of PCAB-*b*-CPEG-90 Films via Vapor-Assisted Alignment. A 2.5 mL solution of PCAB-*b*-CPEG in toluene (3 wt %) was drop-cast on a glass slide and placed under 90% RH until the complete evaporation of toluene solvent at ambient temperature. This process took about 2 h in total. Then, the resulting films were vacuum-dried at 30 °C for 4 h and peeled off from the substrate. The amount of water in the film was examined by thermogravimetric analysis (TGA). The result indicated that there was almost no water associated with PEG in the PCAB-*b*-CPEG (see Figure S12 in the Supporting Information). The films of PCAB-*r*-CPEG-90 and PCAB-90 were prepared by similar procedures.

4.6. Experimental Setup and Method for Humidity-Responsive Deformation Experiment. An acrylic box (90 × 90 × 90 mm) with a round hole (d = 10 mm) on one wall served as a moisture chamber. The entire apparatus was enclosed within a fume cupboard to keep the humidity outside of the moisture chamber stable (approximately RH = 40% at 25 °C). A film with the same shape but without humidity responsibility served as the control group to make sure that the flow could not generate nonresponsive deformation of the film.

In the experiment of deformation under humidity gradients, the sample was positioned vertically near the hole to minimize the impact

https://doi.org/10.1021/acsami.4c01809
ACS Appl. Mater. Interfaces 2024, 16, 15405−15415

of gravity during the experiment. Real-time monitoring of RH inside the chamber (near the hole) and outside the chamber (near the film) allowed for the observation of the humidity gradient. Then, the humidity gradient gradually increases. Once the hygrometer readings stabilized, both the bending angles of the sample and the humidity gradient were recorded.

In the experiment involving deformation under uniformly changed ambient humidity, the film was also positioned vertically inside the chamber, and the humidity inside the chamber was monitored in real time. Subsequently, the RH inside the chamber gradually changed from low to high. After the reading of the hygrometer stabilized, the bending angle of the sample and the real-time humidity were recorded.

4.7. Preparation of Spiral Actuators. The PCAB-*b*-CPEG films were tailored into strips (50 mm × 5 mm × 20 μm). The top and bottom surfaces of the film were marked separately, and the strips were sandwiched between two pieces of thin clean copper. The combined strips were wrapped around a stick and fixed to create the spiral structures. Then, both the stick and combined strips were placed in an oven at 40 °C for 12 h to fix the spiral structures. Finally, the PCAB-*b*-CPEG strips were gently peeled off from the copper to obtain the spiral actuators.

4.8. Measurements. ^{1}H NMR spectra of the monomers and LCPs were recorded on a Bruker AVANCE III NMR spectrometer (400 MHz) using tetramethylsilane (TMS) as the internal standard and $CDCl_3$ as the solvent. The molecular weights of the polymers and their polydispersity indices were measured by a GPC (Waters, e2695) using THF as the mobile phase and polystyrene as the external standard. The thermodynamic properties of all obtained polymers were characterized by DSC (TA, Q2000) at a scanning rate of 10 °C min^{-1} from −20 to 150 °C under nitrogen. The mass loss of LCP during heating was measured by TGA (TA, Q500) at a heating rate of 5 °C min^{-1} from 50 to 600 °C. The texture of the LCP was observed by a POM (Leika, DM2500p) equipped with a Mettler hot stage (models FP-90 and FP-82). 2D-WAXD measurement was conducted on a Xeuss 2.0 System (Xenocs, France) at ambient temperature. The X-ray source consisted of a CuKα with a wavelength of 0.154 nm. Pilatus 3R 200 K-A detector was used to collect two-dimensional (2D) scattering patterns with the sample-to-detector distance set to 140 mm. The peak positions were calibrated with silicon ($2\theta > 15°$) and silver behenate ($2\theta < 10°$), and background scattering was recorded and subtracted from the sample patterns. Surface and cross-sectional SEM images were obtained from Zeiss Sigma 300 field emission scanning electron microscopy (FESEM) at a 5 kV electron beam. All cross-sectional samples were fractured after being dipped into liquid nitrogen.

■ ASSOCIATED CONTENT

Supporting Information

The Supporting Information is available free of charge at https://pubs.acs.org/doi/10.1021/acsami.4c01809.

^{1}H NMR of monomer CPEG; ^{1}H NMR, GPC, and POM images of PCAB-*b*-CPEG; 2D-WAXD images of PCAB-*b*-CPEG films prepared at different humidity; ^{1}H NMR of PCAB-*r*-CPEG; 1D-WAXD results of PCAB-*b*-CPEG and PCAB-*r*-CPEG; DSC of PCAB-*b*-CPEG-90, PCAB-*r*-CPEG-90; photos of static water contact angles of the bottom surface and top surface of PCAB-*b*-CPEG-90 films; 2D-WAXD images of as-prepared PCAB-*r*-CPEG-90 film and PCAB-*r*-CPEG-90 film after vacuum drying; 2D-WAXD image of PCAB-*r*-CPEG-90 film with the thickness of 50 μm; temperature of PCAB-*b*-CPEG-90 films with different irradiation time under varying intensity of UV irradiation; 2D-WAXD images of PCAB-*b*-CPEG-90 film and PCAB-*r*-CPEG-90 film heated to 60 and 90 °C measured at room temperature; TGA curve of PCAB-*b*-CPEG-90 at a heating rate of 5 °C min^{-1}; 2D-WAXD images of the PCAB-*r*-CPEG-90 before and after 20 photodeformation cycles; cross-sectional SEM images of PCAB-*b*-CPEG-90, PCAB-*b*-CPEG-60, PCAB-*r*-CPEG-90, PCAB-90, PCAB-*r*-CPEG-60, PCAB-*r*-CPEG-70, PCAB-*r*-CPEG-80, PCAB-*r*-CPEG-90; and photodeformation of PCAB-*r*-CPEG-60 film and PCAB-*r*-CPEG-60 film exposed to 90% RH for 2 h (PDF)

Reversible photodeformation of PCAB-*b*-CPEG-90 film; the film was irradiated by UV light (365 nm, 35 mW cm^{-2}) for 60 s, and then irradiated by visible light (530 nm, 50 mW cm^{-2}) for 40 s to complete one deformation cycle (MP4)

Photoresponsive deformation of artificial flower actuator; the actuator was irradiated right above the actuator. The flower opened upon UV irradiation and closed under visible light (MP4)

Humidity-responsive deformation of spiral actuators; the outer surface of the actuator was more hydrophilic, and the spiral curled when the ambient humidity was rising (MP4)

Humidity-responsive deformation of spiral actuators; the inner surface of the actuator was more hydrophilic, thus the spiral actuator was uncurled under the high humidity environment (MP4)

Dual-responsive smart "blind" is driven by photo and humidity stimuli (MP4)

Humidity-responsive deformation of artificial flower actuator; artificial flower closed with the increasing ambient humidity from 60% RH to 90% RH, showing the integral control of humidity stimulation (MP4)

Photoresponsive deformation of artificial flower under high humidity; petals of flower were irradiated by the UV light spot one by one, showing the local and precise control of photostimulation (MP4)

■ AUTHOR INFORMATION

Corresponding Author

Jia Wei − *Department of Materials Science, Fudan University, Shanghai 200433, China;* orcid.org/0000-0001-6749-8593; Email: weijia@fudan.edu.cn

Authors

Haozhe Sun − *Department of Materials Science, Fudan University, Shanghai 200433, China*

Xingpeng Chai − *Department of Materials Science, Fudan University, Shanghai 200433, China*

Haipeng Yang − *Department of Materials Science, Fudan University, Shanghai 200433, China*

Yanlei Yu − *Department of Materials Science, Fudan University, Shanghai 200433, China;* orcid.org/0000-0002-4623-3331

Complete contact information is available at: https://pubs.acs.org/10.1021/acsami.4c01809

Author Contributions

All authors have given approval to the final version of the manuscript.

Notes

The authors declare no competing financial interest.

https://doi.org/10.1021/acsami.4c01809
ACS Appl. Mater. Interfaces 2024, 16, 15405−15415

■ ACKNOWLEDGMENTS

The authors would like to acknowledge the financial support from the National Natural Science Foundation of China (52233001, 51927805, 52073062) and Innovation Program of Shanghai Municipal Education Commission (2023ZKZD07).

■ REFERENCES

(1) Ikeda, T.; Mamiya, J.; Yu, Y. Photomechanics of Liquid-Crystalline Elastomers and Other Polymers. *Angew. Chem., Int. Ed.* **2007**, *46* (4), 506−528.
(2) Zhang, Q. M.; Serpe, M. J. Stimuli-Responsive Polymers for Actuation. *ChemPhysChem* **2017**, *18* (11), 1451−1465.
(3) White, T. J. Photomechanical Effects in Liquid Crystalline Polymer Networks and Elastomers. *J. Polym. Sci., Part B: Polym. Phys.* **2018**, *56* (9), 695−705.
(4) Pang, X.; Lv, J. A.; Zhu, C.; Qin, L.; Yu, Y. Photodeformable Azobenzene-Containing Liquid Crystal Polymers and Soft Actuators. *Adv. Mater.* **2019**, *31* (52), No. 1904224.
(5) Stoychev, G.; Kirillova, A.; Ionov, L. Light-Responsive Shape-Changing Polymers. *Adv. Opt. Mater.* **2019**, *7* (16), No. 1900067.
(6) Dong, L.; Zhao, Y. Photothermally Driven Liquid Crystal Polymer Actuators. *Mater. Chem. Front.* **2018**, *2* (11), 1932−1943.
(7) Shang, Y.; Wang, J.; Ikeda, T.; Jiang, L. Bio-Inspired Liquid Crystal Actuator Materials. *J. Mater. Chem. C* **2019**, *7* (12), 3413−3428.
(8) Urayama, K. Switching Shapes of Nematic Elastomers with Various Director Configurations. *React. Funct. Polym.* **2013**, *73* (7), 885−890.
(9) Li, Y.; Ambrogi, V.; Cerruti, P.; Goswami, M.; Yang, Z.; Kessler, M. R.; Rios, O. Functional Liquid Crystalline Epoxy Networks and Composites: From Materials Design to Applications. *Int. Mater. Rev.* **2022**, *67* (2), 201−229.
(10) Dai, M.; Picot, O. T.; Verjans, J. M.; de Haan, L. T.; Schenning, A. P. H. J.; Peijs, T.; Bastiaansen, C. W. Humidity-Responsive Bilayer Actuators Based on a Liquid-Crystalline Polymer Network. *ACS Appl. Mater. Interfaces* **2013**, *5* (11), 4945−4950.
(11) de Haan, L. T.; Verjans, J. M.; Broer, D. J.; Bastiaansen, C. W.; Schenning, A. P. H. J. Humidity-Responsive Liquid Crystalline Polymer Actuators with an Asymmetry in the Molecular Trigger That Bend, Fold, and Curl. *J. Am. Chem. Soc.* **2014**, *136* (30), 10585−10588.
(12) Ryabchun, A.; Lancia, F.; Nguindjel, A. D.; Katsonis, N. Humidity-Responsive Actuators from Integrating Liquid Crystal Networks in an Orienting Scaffold. *Soft Matter* **2017**, *13* (44), 8070−8075.
(13) Kim, K.; Guo, Y.; Bae, J.; Choi, S.; Song, H. Y.; Park, S.; Hyun, K.; Ahn, S. K. 4d Printing of Hygroscopic Liquid Crystal Elastomer Actuators. *Small* **2021**, *17* (23), No. 2100910.
(14) Lugger, S. J. D.; Houben, S. J. A.; Foelen, Y.; Debije, M. G.; Schenning, A. P. H. J.; Mulder, D. J. Hydrogen-Bonded Supramolecular Liquid Crystal Polymers: Smart Materials with Stimuli-Responsive, Self-Healing, and Recyclable Properties. *Chem. Rev.* **2022**, *122* (5), 4946−4975.
(15) Zhang, Y.; Zhang, C.; Wang, R.; Tan, W.; Gu, Y.; Yu, X.; Zhu, L.; Liu, L. Development and Challenges of Smart Actuators Based on Water-Responsive Materials. *Soft Matter* **2022**, *18* (31), 5725−5741.
(16) Davidson, Z. S.; Shahsavan, H.; Aghakhani, A.; Guo, Y.; Hines, L.; Xia, Y.; Yang, S.; Sitti, M. Monolithic Shape-Programmable Dielectric Liquid Crystal Elastomer Actuators. *Sci. Adv.* **2019**, *5* (11), No. eaay0855.
(17) Petsch, S.; Rix, R.; Khatri, B.; Schuhladen, S.; Müller, P.; Zentel, R.; Zappe, H. Smart Artificial Muscle Actuators: Liquid Crystal Elastomers with Integrated Temperature Feedback. *Sensors Actuat. A-Phys.* **2015**, *231*, 44−51.
(18) Schuhladen, S.; Preller, F.; Rix, R.; Petsch, S.; Zentel, R.; Zappe, H. Iris-Like Tunable Aperture Employing Liquid-Crystal Elastomers. *Adv. Mater.* **2014**, *26* (42), 7247−7251.
(19) Spillmann, C. M.; Naciri, J.; Ratna, B. R.; Selinger, R. L.; Selinger, J. V. Electrically Induced Twist in Smectic Liquid-Crystalline Elastomers. *J. Phys. Chem. B* **2016**, *120* (26), 6368−6372.
(20) Roach, D. J.; Kuang, X.; Yuan, C.; Chen, K.; Qi, H. J. Novel Ink for Ambient Condition Printing of Liquid Crystal Elastomers for 4d Printing. *Smart Mater. Struct.* **2018**, *27* (12), No. 125011.
(21) Filipcsei, G.; Csetneki, I.; Szilagyi, A.; Zrinyi, M. Magnetic Field-Responsive Smart Polymer Composites. *Adv. Polym. Sci.* **2007**, *206*, 137−189.
(22) Haberl, J. M.; Sanchez-Ferrer, A.; Mihut, A. M.; Dietsch, H.; Hirt, A. M.; Mezzenga, R. Liquid-Crystalline Elastomer-Nanoparticle Hybrids with Reversible Switch of Magnetic Memory. *Adv. Mater.* **2013**, *25* (12), 1787−1791.
(23) Herrera-Posada, S.; Mora-Navarro, C.; Ortiz-Bermudez, P.; Torres-Lugo, M.; McElhinny, K. M.; Evans, P. G.; Calcagno, B. O.; Acevedo, A. Magneto-Responsive Liquid Crystalline Elastomer Nanocomposites as Potential Candidates for Dynamic Cell Culture Substrates. *Mater. Sci. Eng., C* **2016**, *65*, 369−378.
(24) Bisoyi, H. K.; Li, Q. Liquid Crystals: Versatile Self-Organized Smart Soft Materials. *Chem. Rev.* **2022**, *122* (5), 4887−4926.
(25) Sun, D.; Zhang, J.; Li, H.; Shi, Z.; Meng, Q.; Liu, S.; Chen, J.; Liu, X. Toward Application of Liquid Crystalline Elastomer for Smart Robotics: State of the Art and Challenges. *Polymers* **2021**, *13* (11), 1889−1912.
(26) Michal, B. T.; McKenzie, B. M.; Felder, S. E.; Rowan, S. J. Metallo-, Thermo-, and Photoresponsive Shape Memory and Actuating Liquid Crystalline Elastomers. *Macromolecules* **2015**, *48* (10), 3239−3246.
(27) Wang, Y.; Wang, Z.; He, Q.; Iyer, P.; Cai, S. Electrically Controlled Soft Actuators with Multiple and Reprogrammable Actuation Modes. *Adv. Intell. Syst.* **2020**, *2* (6), No. 1900177.
(28) Liu, Z.; Bisoyi, H. K.; Huang, Y.; Wang, M.; Yang, H.; Li, Q. Thermo- and Mechanochromic Camouflage and Self-Healing in Biomimetic Soft Actuators Based on Liquid Crystal Elastomers. *Angew. Chem., Int. Ed.* **2022**, *61* (8), No. e202115755.
(29) Braun, L. B.; Hessberger, T.; Pütz, E.; Müller, C.; Giesselmann, F.; Serra, C. A.; Zentel, R. Actuating Thermo- and Photo-Responsive Tubes from Liquid Crystalline Elastomers. *J. Mater. Chem. C* **2018**, *6* (34), 9093−9101.
(30) Pozo, M.; Liu, L.; Pilz da Cunha, M.; Broer, D. J.; Schenning, A. P. H. J. Direct Ink Writing of a Light-Responsive Underwater Liquid Crystal Actuator with Atypical Temperature-Dependent Shape Changes. *Adv. Funct. Mater.* **2020**, *30* (50), No. 2005560.
(31) Liu, Q.; Zhan, Y.; Wei, J.; Ji, W.; Hu, W.; Yu, Y. Dual-Responsive Deformation of a Crosslinked Liquid Crystal Polymer Film with Complex Molecular Alignment. *Soft Matter* **2017**, *13* (36), 6145−6151.
(32) Boothby, J. M.; Ware, T. H. Dual-Responsive, Shape-Switching Bilayers Enabled by Liquid Crystal Elastomers. *Soft Matter* **2017**, *13* (24), 4349−4356.
(33) Feng, C.; Rajapaksha, C. P. H.; Cedillo, J. M.; Piedrahita, C.; Cao, J.; Kaphle, V.; Lussem, B.; Kyu, T.; Jakli, A. Electroresponsive Ionic Liquid Crystal Elastomers. *Macromol. Rapid Commun.* **2019**, *40* (19), No. 1900299.
(34) Pilz da Cunha, M.; Foelen, Y.; Raak, R. J. H.; Murphy, J. N.; Engels, T. A. P.; Debije, M. G.; Schenning, A. P. H. J. An Untethered Magnetic- and Light-Responsive Rotary Gripper: Shedding Light on Photoresponsive Liquid Crystal Actuators. *Adv. Opt. Mater.* **2019**, *7* (7), No. 1801643.
(35) Verpaalen, R. C. P.; Souren, A. E. J.; Debije, M. G.; Engels, T. A. P.; Bastiaansen, C. W. M.; Schenning, A. P. H. J. Unravelling Humidity-Gated, Temperature Responsive Bilayer Actuators. *Soft Matter* **2020**, *16* (11), 2753−2759.
(36) Liu, Y.; Xu, B.; Sun, S.; Wei, J.; Wu, L.; Yu, Y. Humidity- and Photo-Induced Mechanical Actuation of Cross-Linked Liquid Crystal Polymers. *Adv. Mater.* **2017**, *29* (9), No. 1604792.
(37) Wani, O. M.; Verpaalen, R.; Zeng, H.; Priimagi, A.; Schenning, A. P. H. J. An Artificial Nocturnal Flower Via Humidity-Gated

Photoactuation in Liquid Crystal Networks. *Adv. Mater.* **2019**, *31* (2), No. 1805985.
(38) Herbert, K. M.; Fowler, H. E.; McCracken, J. M.; Schlafmann, K. R.; Koch, J. A.; White, T. J. Synthesis and Alignment of Liquid Crystalline Elastomers. *Nat. Rev. Mater.* **2022**, *7* (1), 23−38.
(39) Finkelmann, H.; Happ, M.; Portugal, M.; Ringsdorf, H. Liquid Crystalline Polymers with Biphenyl-Moieties as Mesogenic Group. *Makromol. Chem.* **1978**, *179* (10), 2541−2544.
(40) Finkelmann, H.; Ringsdorf, H.; Wendorff, J. H. Model Considerations and Examples of Enantiotropic Liquid Crystalline Polymers. *Makromol. Chem.* **1978**, *179* (1), 273−276.
(41) Yu, Z. Q.; Li, T. T.; Zhang, Z.; Liu, J.-H.; Yuan, W. Z.; Lam, J. W. Y.; Yang, S.; Chen, E.-Q.; Tang, B. Z. Phase Behaviors of Side-Chain Liquid Crystalline Polyacetylenes with Different Length of Spacer: Where Will the Decoupling Effect Appear? *Macromolecules* **2015**, *48* (9), 2886−2893.
(42) Lv, J. A.; Liu, Y.; Wei, J.; Chen, E.; Qin, L.; Yu, Y. Photocontrol of Fluid Slugs in Liquid Crystal Polymer Microactuators. *Nature* **2016**, *537* (7619), 179−184.
(43) Liu, Q.; Liu, Y.; Lv, J. A.; Chen, E.; Yu, Y. Photocontrolled Liquid Transportation in Microtubes by Manipulating Mesogen Orientations in Liquid Crystal Polymers. *Adv. Intell. Syst.* **2019**, *1* (6), No. 1900060.
(44) Xu, B.; Zhu, C.; Qin, L.; Wei, J.; Yu, Y. Light-Directed Liquid Manipulation in Flexible Bilayer Microtubes. *Small* **2019**, *15* (24), No. 1901847.
(45) Han, S.; Chen, Y.; Xu, B.; Wei, J.; Yu, Y. An Azoester-Containing Photoresponsive Linear Liquid Crystal Polymer with Good Mesophase Stability. *Chin. J. Polym. Sci.* **2020**, *38* (8), 806−813.
(46) Ware, T. H.; Perry, Z. P.; Middleton, C. M.; Iacono, S. T.; White, T. J. Programmable Liquid Crystal Elastomers Prepared by Thiol-Ene Photopolymerization. *ACS Macro Lett.* **2015**, *4* (9), 942−946.
(47) Aharoni, H.; Xia, Y.; Zhang, X.; Kamien, R. D.; Yang, S. Universal Inverse Design of Surfaces with Thin Nematic Elastomer Sheets. *Proc. Natl. Acad. Sci. U.S.A.* **2018**, *115* (28), 7206−7211.
(48) Zhao, X.; Chen, Y.; Peng, B.; Wei, J.; Yu, Y. L. A Facile Strategy for the Development of Recyclable Multifunctional Liquid Crystal Polymers Via Post-Polymerization Modification and Ring-Opening Metathesis Polymerization. *Angew. Chem., Int. Ed.* **2023**, *62*, No. e202300699.
(49) Zheng, X.; Guan, S.; Zhang, C.; Qu, T.; Wen, W.; Zhao, Y.; Chen, A. A Cut-and-Weld Process to 3d Architectures from Multiresponsive Crosslinked Liquid Crystalline Polymers. *Small* **2019**, *15* (16), No. 1900110.

https://doi.org/10.1021/acsami.4c01809
ACS Appl. Mater. Interfaces 2024, 16, 15405−15415